Submicron Particle Mass Concentrations and Sources in the Amazonian Wet Season (AMAZE-08)

Q. Chen[1,*], D. K. Farmer[2,**], L. V. Rizzo[3], T. Pauliquevis[3], M. Kuwata[1,***], T. G. Karl[4,****], A. Guenther[4,*****], J. D. Allan[5], H. Coe[5], M. O. Andreae[6], U. Pöschl[6], J. L. Jimenez[2], P. Artaxo[7], S. T. Martin[1]

(1) School of Engineering and Applied Sciences & Department of Earth and Planetary Sciences, Harvard University, Cambridge, MA, USA
(2) Department of Chemistry and Biochemistry & Cooperative Institute for Research in Environmental Science, University of Colorado, Boulder, CO, USA
(3) Department of Exact and Earth Sciences, Federal University of São Paulo, Diadema, Brazil
(4) National Center for Atmospheric Research, Boulder, CO, USA
(5) National Centre for Atmospheric Science & School of Earth, Atmospheric and Environmental Sciences, University of Manchester, Manchester, UK
(6) Max Planck Institute for Chemistry, Mainz, Germany
(7) Applied Physics Department & Atmospheric Science Department, University of São Paulo, São Paulo, Brazil

[*]Now at State Key Joint Laboratory of Environmental Simulation and Pollution Control, College of Environmental Sciences and Engineering, Peking University, Beijing, 100871, China

[**]Now at Department of Chemistry, Colorado State University, Fort Collins, CO, USA

[***] Now at Nanyang Technological University and Earth Observatory of Singapore, Singapore

[****]Now at Institute of Meteorology and Geophysics, University of Innsbruck, Austria

[*****]Now at Atmospheric Sciences and Global Change Division, Pacific Northwest National Laboratory, Richland, WA, USA.

Manuscript submitted to *Atmospheric Chemistry and Physics*

Correspondence to: S.T. Martin (scot_martin@harvard.edu) and P. Artaxo (artaxo@if.usp.br)

Abstract

Real-time mass spectra of the non-refractory species in submicron aerosol particles were recorded in a tropical rainforest in the central Amazon basin during the wet season from February to March 2008, as a part of the Amazonian Aerosol Characterization Experiment (AMAZE-08). Organic material accounted on average for more than 80% of the non-refractory submicron particle mass concentrations during the period of measurements. There was insufficient ammonium to neutralize sulfate. In this acidic, isoprene-rich, HO_2-dominant environment positive-matrix factorization of the time series of particle mass spectra identified four statistical factors to account for the 99% variance of the signal intensities of the organic constituents. The first factor was identified as associated with regional and local pollution and labeled as "HOA" for its hydrocarbon-like characteristics. A second factor was associated with long-range transport and labeled as "OOA-1" for its oxygenated characteristics. A third factor, labeled "OOA-2," was implicated as associated with the reactive uptake of isoprene oxidation products, especially of epoxydiols to acidic haze, fog or cloud droplets. A fourth factor, labeled as "OOA-3," was consistent with an association to the fresh production of secondary organic material (SOM) by a mechanism of gas-phase oxidation of biogenic volatile organic precursors followed by gas-to-particle conversion of the oxidation products. The suffixes 1, 2, and 3 on the OOA labels signify ordinal ranking with respect to the extent of oxidation represented by the factor. The process of aqueous-phase oxidation of water-soluble products of gas-phase photochemistry might also have been associated to some extent with the OOA-2 factor. The campaign-average factor loadings were in a ratio of 1.4:1 for OOA-2:OOA-3, suggesting the comparable importance of particle-phase compared to gas-phase pathways for the production of SOM during the study period.

1. Introduction

Aerosol particles in the atmosphere make an important contribution to the Earth's radiation budget (IPCC, 2013). They can directly scatter and absorb shortwave and longwave radiation, and they can indirectly affect radiative forcing and precipitation by modifying cloud properties. The assessment of the impact of human perturbations on climate requires an understanding of the natural functioning of the aerosol-cloud-climate system. During the wet season, the pristine Amazon basin provides a unique environment for studying the sources and atmospheric evolution of natural aerosol particles and hence understanding the role of aerosol particles in biosphere-atmosphere interactions (Andreae, 2007; Martin et al., 2010a).

Tropical forest emissions and long-range transport from outside of the basin are major contributors to the number and mass budgets of Amazonian aerosol particles during the wet season because regional biomass burning emission is largely suppressed by heavy rainfall (Martin et al., 2010a). The forest ecosystem emits biogenic volatile organic compounds (BVOCs) that can be oxidized in the atmosphere, principally by reaction with photochemically produced hydroxyl radical and ozone molecules. Some of the oxidized products have sufficiently low vapor pressures to condense and produce SOM in the particle phase. Moreover, in haze, fog, and cloud droplets, the production of organic acids and oligomers can occur from the OH-initiated aqueous-phase oxidation of the photooxidation products of isoprene, e.g., glyoxal, methacrolein (MACR), and methylvinyl ketone (MVK) (Lim et al., 2010), as well as from the acid-catalyzed reactive uptake of epoxydiol isomers (IEPOX) (Surratt et al., 2010; Lin et al., 2012). For SOM produced by these aqueous-phase pathways, a fraction of the mass can remain in the particle phase after dehumidification. In addition, the forest also directly emits primary biological particles containing potassium, phosphorus, sugars, sugar alcohols, and fatty acids,

including an upper limit of a 20% contribution to the submicron organic mass concentration (Graham et al., 2003a; Elbert et al., 2007; Schneider et al., 2011; Pöhlker et al., 2012). The forest also emits gases important to the particle mass concentrations of inorganic ions. For example, ammonia partitions from the gas phase to acidic particles (Trebs et al., 2005). Reduced sulfur gases undergo atmospheric oxidation to produces sulfuric acid that condenses to the particle phase (Andreae et al., 1990).

The Amazonian Aerosol Characterization Experiment 2008 (AMAZE-08) investigated the sources and properties of Amazonian particles (Martin et al., 2010b). Evidence from AMAZE-08 led to the conclusion that there is a large-scale contribution of biogenic SOM to the mass concentration of submicron aerosol particles during the wet season (Chen et al., 2009; Martin et al., 2010b; Pöschl et al., 2010; Schneider et al., 2011). In particular, Chen et al. (2009) demonstrated that on order of 90% of the organic material of submicron Amazonian particles arises from the in-Basin production of biogenic SOM. Primary biogenic particles enriched in potassium salts and emitted by fungal spores as 10 to 20 nm dried particles possibly provide surfaces for the condensation of SOM from the gas phase (Pöhlker et al., 2012). These bio-related particles participate in the regulation of the hydrological cycle of the forest by serving as nuclei for cloud formation and subsequent precipitation (Gunthe et al., 2009; Prenni et al., 2009). In addition to particle production tied to the forest ecosystem, lidar and satellite observations provide evidence of episodic long-range advection of African smoke and Saharan dust (Ben-Ami et al., 2010; Baars et al., 2011). These intrusions are temporally consistent with increases of heavily oxidized organic particles observed by Chen et al. (2009), indicative of long atmospheric residence times, as well as increases in the concentrations of ice nuclei observed by Prenni et al. (2009).

The present study analyzes multiple data sets collected during AMAZE-08 in relation to one another and in the context of the chemistry and properties of submicron particles in the Amazon basin during the wet season. A focus topic is the relative importance of aqueous-phase reactions compared to gas-phase oxidation followed by condensation to the production of SOM mass concentration. The relative importance of these two pathways remains poorly understood (Martin et al., 2010a; Ervens et al., 2011). On the one hand, condensational growth has been reported as an important pathway of the biogenic SOM production (Graham et al., 2003a). On the other hand, a significant role of liquid-phase processing for Amazonian aerosol particles is proposed (Pöhlker et al., 2012). In the current study, positive-matrix factorization of the time series of particle mass spectra is used to identify statistical factors that differ in mass spectral patterns (Zhang et al., 2011). The properties of these factors, in conjunction with the auxiliary data sets, are used to investigate the relative importance of different possible sources of submicron organic material in Amazonia during the wet season.

2. Site and Instrument Description

Ground-based measurements were carried out at a rainforest site during the wet season from 7 February to 13 March 2008 (Martin et al., 2010b). The site (02 °35.68 ´S, 60 °12.56 ´W, 110 m above sea level) is located 60 km NNW of Manaus and faces 1600 km of nearly pristine forest to the east to the Atlantic Ocean. The site was accessed by a 34-km unpaved road from Highway 174 (Fig. S1). The ten-day back trajectories indicated that during the measurement period the air masses mainly originated from the northeast over the Atlantic Ocean in the direction of Cape Verde and the Canary Islands. Air was sampled at the top of a tower (“TT34”; 38.75 m) above the forest canopy (33 m). Instrumentation deployed during AMAZE-08 is described in Martin et al. (2010b).

93 The present study focuses mostly on the statistical analysis of the data sets of an
94 Aerodyne high-resolution Aerosol Mass Spectrometer (HR-AMS) in the context of
95 complementary data sets of other instruments. Mass concentrations were adjusted to standard
96 temperature and pressure (noted as STP; 273.15 K and 10^5 Pa), which were approximately 10%
97 greater than those at calibration conditions (299.3 K and 100591.7 Pa). Details on sampling by
98 the AMS and data analysis are provided in Chen et al. (2009) and Sect. A of the Supplement.
99 The description of other concurrent measurements and the comparisons among the
100 measurements are provided in Sect. B of the Supplement. Table S1 lists the regression
101 coefficients for the multi-instrument data comparison. For a collection efficiency of unity, the
102 AMS data agreed within measurement uncertainty with the other data sets, which is consistent
103 with the understanding that liquid particles do not bounce from the AMS vaporizer (Matthew et
104 al., 2008). Images of filter samples showed that spherical organic particles, appearing as like-
105 liquid droplets, were the main population in the submicron fraction of the ambient particle
106 population for AMAZE-08 (Pöschl et al., 2010).
107 Atomic ratios of oxygen-to-carbon (O:C), hydrogen-to-carbon (H:C), nitrogen-to-carbon
108 (N:C), and sulfur-to-carbon (S:C), as well as the organic-mass-to-organic-carbon (OM:OC)
109 ratios, were calculated from the high-resolution "W-mode" data (Aiken et al., 2008). The ratios
110 were corrected by the method of Canagaratna et al. (2015). The contributions of organonitrates
111 and organosulfates, detected as inorganic nitrate or sulfate ions by the AMS, to the elemental
112 ratios were negligible because of their low mass concentrations (cf. Sect. A of the Supplement).
113 Positive-matrix factorization (PMF) (Paatero and Tapper, 1994) was conducted on the organic
114 mass spectra of the medium-resolution "V-mode" data (*m*/*z* 12 to 220) taken to unit-mass
115 resolution. The analysis used the PMF evaluation panel of Ulbrich et al. (2009) (version 4.2;

"robust mode"). Further aspects of the analysis and output evaluation are provided in Sect. C of the Supplement. Because of the low mass concentrations, the signal-to-noise ratios were insufficient for satisfactory PMF analysis of the high-resolution data. PMF results are reported herein for unit mass resolution.

The AMS mass spectra of SOM produced in the Harvard Environmental Chamber (HEC) by (i) the photooxidation of isoprene (C_5H_8), (ii) the dark ozonolysis of the monoterpene α-pinene ($C_{10}H_{16}$) (adapted from Shilling et al. (2009)), and (iii) the dark ozonolysis of the sesquiterpene β-caryophyllene ($C_{15}H_{24}$) are reported herein for the purpose of comparison to the AMAZE-08 data. Experimental details are described elsewhere (Shilling et al., 2009; King et al., 2010; Chen et al., 2011 and 2012). A library of spectra was collected at different SOM mass concentrations.

3. Results and Discussion

3.1 Mass concentrations

Figure 1 shows a time series of measurements by the AMS and other instruments during AMAZE-08. The AMS detects the non-refractory chemical components of the submicron fraction of the ambient particle population (NR-PM_1) (Fig. 1a-1c). As described in Chen et al. (2009), organic material and sulfate were the two major components identified by the AMS, with correspondingly low concentrations of ammonium and negligible concentrations of nitrate and chloride. The campaign-average organic particle mass concentration was 0.76 ± 0.23 μg m^{-3}, corresponding to 0.45 ± 0.13 μg C m^{-3} of organic carbon and an OM:OC ratio of 1.7. The campaign-average sulfate mass concentration of 0.19 ± 0.06 μg m^{-3} agreed well with the average value of 0.21 ± 0.06 μg m^{-3} measured by ion chromatography (IC) and the value of 0.24 ± 0.05 μg m^{-3} measured by particle-induced X-ray emission (PIXE) for the fine-mode (PM_2) filters.

Ammonium accounted for 2% of the submicron particle mass concentration. The campaign-average mass concentration was 0.03 ± 0.01 μg m^{-3}, in agreement with the average value of 0.04 ± 0.01 μg m^{-3} obtained for the fine-mode filters by the IC analysis. Chloride concentrations, had a campaign-average concentration of 2 ng m^{-3}, which was consistent with the filter average, though there were transiently larger levels (up to 26 ng m^{-3}) during some periods. Nitrate had a campaign-average concentration of 7 ± 2 ng m^{-3}. This value was greater than the average fine-mode concentration of 4 ± 1 ng m^{-3} measured by IC, perhaps because of increased instrument uncertainties at low concentrations. Another possibility, meaning substantial evaporative losses of nitrate during filter sampling, is not anticipated for the hygroscopic, acidic particles present during the measurement periods for the prevailing relative humidity. The AMS-measured nitrate accounted for 0.6% of the total submicron particle mass concentration.

Black carbon, mineral dust, and sea salt are common refractory components that are not quantified by the AMS. The multiangle absorption photometer (MAAP) instrument provides an optically based measurement of the black-carbon-equivalent (BCe) mass concentration, without size resolution (Petzold et al., 2002). The campaign-average concentration was 0.13 μg m^{-3} (Fig. 1d). Under a limiting assumption that all black carbon occurred in the submicron fraction of the atmospheric particle population, this concentration corresponded to 11% of the submicron mass concentration (inset of Fig. 1e). The relative contribution of black carbon varied significantly during the course of AMAZE-08 (Fig. 1e), perhaps corresponding to the occasional advection of urban pollution from Manaus or biomass burning from Africa (Kuhn et al., 2010; Martin et al., 2010b; Rizzo et al., 2013). This interpretation is supported by the covariance of BCe with sulfate. Major fine-mode (PM_2) trace elements of mineral dust, including Si, Al, Fe, and Ca, had campaign-average mass concentrations of 0.12, 0.05, 0.04, and 0.01 μg m^{-3}, respectively, as

analyzed for fine-mode filter samples by PIXE. An important source of the mineral dust was long-range transport from Africa. Previous campaigns in the Amazon found that about 20% of the mineral dust occurred in the submicron domain (Fuzzi et al., 2007). Using this result for AMAZE-08 implies that mineral dust contributed about 0.1 $\mu g\ m^{-3}$ to the average mass concentration of the submicron particle population (Malm et al., 1994). The modified pie chart is shown in Fig. S2. Moreover, the campaign-average mass concentrations of fine-mode metallic elements (V, Cr, Mn, Ni, Cu, Zn, Pb, and Mg in total of 2 $ng\ m^{-3}$) measured by PIXE were sufficiently low during AMAZE-08 to confirm the absence in the submicron particle mass concentration of significant metals from anthropogenic sources. The campaign-average mass concentration of fine-mode Na^+ measured by IC was 0.02 $\mu g\ m^{-3}$. This result suggests a minimal contribution of sea salt from the Atlantic Ocean, at least to the submicron particle population (Fuzzi et al., 2007).

Figure 1f shows the time series of the particle light scattering coefficient measured by nephelometry at 550 nm for PM_7. The elevated scattering coefficients during 22 February to 3 March 2008 were driven by elevated mineral dust concentrations in the coarse mode, along with elevated submicron sulfate, BCe, and organic material arising from the advection of the Manaus pollution plume as well as long-range transport from Africa (Sect. B of the Supplement). Other temporal maxima corresponded to increases of submicron particle mass concentration. Figure 1g shows the elemental compositions of the submicron organic material measured by the AMS. The O:C and H:C ratios, corrected as described in Canagaratna et al. (2015), were 0.58 ± 0.16 (one standard deviation) and 1.60 ± 0.18, on average, respectively. The 10/90 quantiles were 0.40/0.74 and 1.42/1.80, respectively. The N:C ratios were 0.03 ± 0.01.

Ammonium and sulfate mass concentrations had high correlation ($R^2 = 0.95$) during

AMAZE-08 (Fig. S3). The molar ratio of $NH_4^+ : SO_4^{2-}$ was 0.80 (Fig. 2), meaning that there was insufficient ammonium to neutralize sulfate for the submicron particle population and suggesting a composition close to that of ammonium bisulfate. Similar molar ratios have been reported in several previous studies in the central and northeast Amazon basin (Talbot et al., 1988, 1990; Gerab et al., 1998; Graham et al., 2003b). The AMS is unable to quantify refractory components such as K^+, Na^+, Ca^{2+}, and Mg^{2+}. Mass-diameter distributions of these ions obtained by IC analysis of samples collected by a Multi-Orifice Uniform Deposit Impactor (MOUDI) on 22 March 2008 suggest that 40% of the mass of these ions was distributed to the submicron particle fraction. For comparison, Fuzzi et al. (2007) for the wet season reported 50-60% of K^+ and Ca^{2+} in the submicron fraction, compared to the predominance of Na^+ and Mg^{2+} in the supermicron fraction. The campaign-average fine-mode mass concentrations of K^+, Ca^{2+}, Na^+, and Mg^{2+} measured by IC were 0.03, 0.01, 0.02, and 0.01 $\mu g\ m^{-3}$, respectively. The implication of the relative concentrations (i.e., sulfate concentration of $0.19 \pm 0.06\ \mu g\ m^{-3}$) is that the submicron inorganic ion composition is reasonably approximated as ammonium bisulfate during AMAZE-08.

Diel profiles of organic, sulfate, ammonium, nitrate, and chloride mass concentrations measured by the AMS are shown in Fig. 3. The temporal trends of the four species were correlated, with a minimum in mass concentrations near daybreak and a maximum in the afternoon. Nighttime rainfall efficiently removed particle mass concentration after local midnight, suggesting an absence of strong sources of submicron particles during the night. From the morning to the afternoon, photochemical production of SOM, convective mixing of particles from aloft, and regional advection sustained mass concentrations, with quick recovery after daytime rainfall. Precipitation was typically local whereas advection was typically regional at a

larger scale than precipitation. The decrease and the recovery of species concentration during the afternoon resulted from frequent rain events around that time of day (e.g., Fig. S4). The organic particle mass concentration increased during the day even as temperature rose and relative humidity dropped, both of which provide a thermodynamic driving force for the re-partitioning of semivolatile species from the particle phase to the gas phase (Pankow, 1994). Possible explanations include (1) sufficiently strong daytime production of SOM to outweigh evaporative sinks, (2) significant production of low-volatility SOM (Ervens et al., 2011; Ehn et al., 2014), or (3) a slow evaporation rate of SOM (Vaden et al., 2011).

3.2. Mass spectra of laboratory biogenic SOM

As a reference for interpreting the AMAZE-08 measurements, Figure 4 shows the mass spectra of SOM produced in the HEC by the oxidation of isoprene, α-pinene, and β-caryophyllene for three different mass concentrations. Signals at $m/z < 60$ account for 93-97%, 80-84%, and 71-79% of the total signal intensity for the three types of SOM. The fragmentation pattern extends to higher m/z for the increasing carbon skeleton of precursor BVOC. For all three types of SOM, the relative intensities of two prominent ions, $C_2H_3O^+$ at m/z 43 and CO_2^+ at m/z 44, show opposite trends as the mass concentration increases. The former increases for elevated concentrations whereas the later decreases. Another ion at m/z 44, $C_2H_4O^+$, shows a trend similar to that of $C_2H_3O^+$. This ion accounts for 10−25%, 3−5%, and 5−10% of the signal at m/z 44 for the isoprene, α-pinene, and β-caryophyllenethe SOMs, respectively. The relative intensities of major $C_xH_y^+$ ions, such as CH_3^+ at m/z 15, $C_2H_3^+$ at m/z 27, $C_3H_3^+$ at m/z 39, and $C_3H_5^+$ at m/z 41, typically increase as concentration increases. The most intense $C_xH_y^+$ ions at $m/z >$ 80 for the three types of biogenic SOM is $C_7H_7^+$ at m/z 91, which does not occur in the spectra for fresh emissions such as diesel exhaust, cooking, and biomass burning but is similar to the spectra

231 for aged primary emissions (Chirico et al., 2010; He et al., 2010; Ortega et al., 2013).

232 Compared to the spectra of the other types of biogenic SOM, isoprene-derived SOM
233 under HO_2-dominant conditions has a unique signature. "HO_2-dominant" refers to the fate of
234 peroxy radicals with respect to reaction with HO_2 or NO. The relative intensities of CHO^+ at *m*/*z*
235 29, CH_2O^+ at *m*/*z* 30, CH_3O^+ at *m*/*z* 31, $C_3H_6O_2^+$ at *m*/*z* 74, and $C_3H_7O_2^+$ at *m*/*z* 75 in the spectra
236 of isoprene-derived SOM are much greater, and the contributions of $C_xH_y^+$ ions are less,
237 especially for *m*/*z* > 65. Moreover, *m*/*z* 82 that mainly consists of $C_3H_5O^+$ appears to be the most
238 intense peak for $m/z \geq 75$. This fragment has been suggested as a characteristic fragment of
239 isoprene-derived SOM (Robinson et al., 2011). Isoprene-derived SOM also does not follow the
240 empirical linear relationship between O:C and I_{44}:I_{org} described by Aiken et al. (2008) (Fig. S5),
241 indicating that deriving O:C from I_{44}:I_{org} requires careful judgments on the contribution of
242 isoprene-derived SOM.

243 3.3 Multivariate factor analysis of the organic mass spectra

244 Multivariate analysis by PMF of the temporal series of the organic component of the
245 mass spectra was carried out for $12 \leq m/z \leq 220$ at unit-mass resolution. In overview, four
246 statistical factors were identified and labeled as HOA, OOA-1, OOA-2, and OOA-3 (Fig. 5).
247 These four factors respectively accounted for 2%, 18%, 14%, and 66% of the variance in the data
248 matrix, with a residual variance of <1%. The time series of the loading of each statistical factor
249 are shown in Fig. 6. By definition, the mass spectrum of the organic chemical component itself
250 was at any time point a linear mix of the statistical factors, plus residual.

251 The HOA factor (Fig. 5a) was dominated by the ion series $C_nH_{2n+1}^+$, $C_nH_{2n-1}^+$, and $C_nH_{2n-3}^+$
252 (*m*/*z* 27, 29, 39, 41, 43, 55, 57, 67, 69…), similar to that reported for other locations (e.g., Zhang
253 et al., 2005; Docherty et al., 2011; Robinson et al., 2011) and to that observed for engine exhaust

(Canagaratna et al., 2004; Chirico et al., 2010). This statistical factor is typically taken as an organic component associated with fossil fuel combustion emissions that have not undergone substantial atmospheric oxidation. This factor was especially prevalent in the early part of the experiment. During this time period, other pollution tracers such as sulfate and NO_x were also at elevated concentrations. Regional pollution from Manaus and local emissions (e.g., nearby roads, highway, generator, and pump oil) were plausible contributors to the loading of the HOA factor (Ahlm et al., 2009; Rizzo et al., 2013).

The factors OOA-1, OOA-2, and OOA-3 were ranked by the f_{44}:f_{43} ratios (high to low) and labeled based on Zhang et al. (2011), where $f_{m/z}$ represents the fractional contribution of the signal intensity at *m*/*z* to the statistical factor. The signal intensity was dominated at *m*/*z* 44 by the CO_2^+ fragment and at *m*/*z* 43 by the $C_2H_3O^+$ and $C_3H_7^+$ fragments. The f_{44}:f_{43} ratio has been used in some settings as a surrogate for the extent of oxidation (i.e., so-called 'atmospheric aging') of SOM (Ng et al., 2010 and 2011).

The OOA-1 factor had the feature of a singularly dominant peak at *m*/*z* 44 (Fig. 5b).This marker has been linked to organic material that has undergone extensive oxidation during a prolonged atmospheric residence time (on the order of 10 days) (Ng et al., 2010; Lambe et al., 2011). This factor is consistent with an association to finding of highly-oxidized organic material delivered by long-range transport, as occurred during some periods of AMAZE-08 (Chen et al., 2009). The source of this material was plausibly African biomass burning, as supported by concurrent lidar measurements (Baars et al., 2011) and satellite observations (Ben-Ami et al., 2010). Biomass burning in South America was much less significant during the wet season (Martin et al., 2010b). The correlations of the statistical loadings of the OOA-1 factor with the measured mass concentrations of biomass burning tracers, such as chloride (R^2 = 0.52),

277 potassium (R^2 = 0.35), and black carbon (R^2 = 0.43) in the submicron particle population, were
278 not high, possibly because of the mixing of sources to these tracers such as primary biological
279 particles (i.e., contributing chloride and potassium) and regional pollution from Manaus to (i.e.,
280 black carbon). These correlation values were, however, significantly greater than those of the
281 other three factors (HOA, OOA2, and OOA-3) with the tracers (i.e., $R^2 < 0.10$ for chloride, $R^2 <$
282 0.02 for potassium, and $R^2 < 0.20$ for black carbon) (Fig. 6b). Elevated sulfate mass
283 concentrations were also observed during periods having high OOA-1 loadings (Fig. 1b).
284 Features of the OOA-2 factor included (1) a f_{44}:f_{43} ratio greater than unity and (2) a
285 characteristic peak at *m*/*z* 82 mainly consisting of $C_3H_5O^+$. This peak was the most abundant for
286 $m/z \geq 75$ (Fig. 5c). It is similar to that reported for PMF factors identified in the tropical
287 rainforest of Borneo (named as the "82Fac" factor) (Robinson et al., 2011), the rural area of
288 southwest Ontario, Canada (named as the "UNKN" factor) (Slowik et al., 2011), and isoprene-
289 rich downtown Atlanta, Georgia, USA (named as the "IEPOX-OA" factor) (Budisulistiorini et
290 al., 2013). Robinson et al. (2011) concluded that this factor derived from SOM produced by
291 isoprene photo-oxidation. In agreement, the time series of OOA-2 loading correlated with
292 isoprene concentration (R^2 = 0.65) as well as with the sum concentration of first-generation
293 isoprene oxidation products, specifically MVK + MACR (R^2 = 0.74) (Fig. 6c). The characteristic
294 *m*/*z* 82 also occurred in the spectra of our isoprene SOM produced in the presence of neutral
295 sulfate particles at 40% RH (Fig. 4a). Laboratory studies demonstrated that the reactive-uptake
296 of photo-oxidation products of isoprene, particularly IEPOX, in the presence of acidic particles
297 contribute to the *m*/*z* 82 signal detected by the AMS (Lin et al., 2012; Budisulistiorini et al.,
298 2013; Liu et al., 2014). Even so, the spectra of isoprene SOM or IEPOX SOM produced in the
299 laboratory have some important differences with the statistical factors (i.e., "OOA-2" of this

study and "82Fac", "UNKN", and "IEPOX-OA" of earlier studies) derived from atmospheric data sets. In particular, there are significant differences at *m*/*z* 29 and *m*/*z* 39 through *m*/*z* 44. The values of f_{44} of the laboratory results are approximately 25% of those of the cited PMF factors. One possible explanation for these differences is that the laboratory experiments did not capture the full range of atmospheric processes, such as possible synergistic chemistry among the range of atmospheric precursors, aqueous-phase processing, and photochemistry under a range of HO_2:NO ratios (Ervens et al., 2011; Emanuelsson et al., 2013; Liu et al., 2013; Nguyen et al., 2014). In particular, the laboratory experiments were typically carried out at low relative humidity. The atmosphere during AMAZE-08 was humid (89 to 100% RH; 25 to 75% quantiles). Pöhlker et al. (2012) showed evidence of multiphase processing in the larger accumulation mode particles. The oxidized material produced by aqueous-phase oxidation (e.g., dicarboxylic acids (Lim et al., 2010)) may explain the higher f_{44} in the OOA-2 factor compared to the laboratory spectra. In summary, the OOA-2 factor during AMAZE-08 was interpreted as SOM produced by the reactive uptake of isoprene photo-oxidation products, including possible aqueous-phase oxidation in haze, fog, and cloud droplets.

The OOA-3 factor had a prominent peak at *m*/*z* 43 (Fig. 5d). For *m*/*z* > 80, the most intense peak occurred at *m*/*z* 91. The OOA-3 factor had similarities to the mass spectra recorded for biogenic SOM produced under conditions relevant to the Amazon basin. Specifically, SOM produced from isoprene under laboratory conditions had a prominent peak at *m*/*z* 43 (Fig. 4a). Mass spectra of SOM derived from precursors of monoterpene α-pinene and sesquiterpene β-caryophyllene had similar patterns as OOA-3 at *m*/*z* 55 and *m*/*z* 91. A linear combination of the three chamber spectra largely reproduced the OOA-3 factor (Fig. 7; 50% isoprene-derived SOM, 30% α-pinene-derived SOM, and 20% β-caryophylene-derived SOM). The intensity at *m*/*z* 29,

however, was overestimated by the linear combination. The remarkable result is that the ambient factor could to large extent be explained by just three laboratory data sets given the wide range of BVOC precursor compounds that can contribute to SOM production in the Amazon basin. The explanation is three-fold, one that isoprene is the dominant BVOC for this rain forest, two that the AMS breaks complex molecules into simpler building blocks by electron-impact ionization, and three that the higher-order C_{10}, C_{15}, and possibly C_{20} BVOCs are all assembled biochemically from the isoprene (C_5) monomer. Moreover, the temporal variation of the OOA-3 loading tracked that of the BVOC concentrations (Fig. 6d). The OOA-3 statistical factor was therefore interpreted as associated with freshly produced SOM similar to that produced in the chamber experiments, meaning on a timescale of several hours by a mechanism of gas-to-particle partitioning of the BVOC oxidation products.

Figure 8 shows the campaign-average diel profiles of the factor loadings. The HOA loading had a daytime minimum, suggesting the buildup of local pollution during the night and the removal by convective mixing during the day. In support of this interpretation, the nocturnal boundary layer was approximately 100 m or less. At daybreak, the boundary layer rapidly developed, reaching on order of 1000 m by local noon around the site (Martin et al., 2010b). The OOA-1 loading peaked around noon without great variation throughout the day. This temporal behavior is expected for homogeneous mixing in the atmospheric column without in situ sources, such as for material arriving by long-range transport. The small daytime increase was consistent with the daytime convective downward mixing of older, oxidized particles from aloft. By comparison, the OOA-2 and OOA-3 loadings peaked in the early afternoon while the BVOC concentrations were high (cf. Fig. 3c of Chen et al. (2009)). This temporal behavior was consistent with the photochemically driven production of SOM.

346 Figure 9 shows the time series of fractional contribution by each of the four statistical
347 factors identified by PMF analysis. On average the relative loadings of HOA, OOA-1, OOA-2,
348 and OOA-3 were 14%, 14%, 34%, and 38%, respectively. For comparison, other studies reported
349 0 to 21% of HOA for remote locations (Jimenez et al., 2009) and 23% to 50% of OOA-2 (named
350 as "82Fac", "UNKN", and "IEPOX-OA" in earlier studies) (Robinson et al., 2011; Slowik et al.,
351 2011; Budisulistiorini et al., 2013). Figure 9 shows that the relative importance of each process
352 as a contributor differed with time and highlights two focus periods. Precipitation and
353 temperature were the major meteorological factors that differed between the two periods. The
354 first period was sunny, warmer with occasional clouds, and the second period had frequent heavy
355 rainfall events. Long-range back-trajectory analyses presented in Martin et al. (2010b) showed
356 that the air masses consistently arrived from the equatorial Atlantic Ocean passing as
357 northeasterlies through the Amazon basin. Local measurements showed that the daytime winds
358 mainly came from the north and northeast (Fig. 9, top). During the first period, the average
359 fractional contribution by the OOA-2 factor was five times greater than that of the OOA-3 factor.
360 During the second period, by comparison, the fractional contribution by the OOA-3 factor was
361 three times greater than that of the OOA-2 factor. The average organic mass concentrations of
362 the two periods were 1.84 and 0.59 $\mu g\ m^{-3}$, respectively.
363 Figure 9 shows that the loading fraction of the OOA-2 factor consistently dropped
364 following heavy rainfall events, suggesting more efficient in-cloud or below-cloud scavenging
365 for the types of material represented by OOA-2 than for those types represented by OOA-3. This
366 finding further supports the interpretation that the OOA-2 factor represents, at least in part,
367 aqueous-phase production pathways because SOM produced in this way has greater water
368 solubility and hence greater wet deposition rates than SOM produced freshly by gas-to-particle

condensation, as interpreted for the OOA-3 factor. Figure 9 also shows that the mode diameter of organic material in period 1, which has a higher OOA-2 loading fraction, is significantly larger than that in period 2, which has a higher OOA-3 loading fraction. Aqueous-phase processing is anticipated to add additional organic material that results in larger mode diameters after dehydration.

4. Conclusions

Submicron particle mass concentration in the Amazonian rainforest during the wet season of 2008 was dominated by organic material. The environment was humid, HO_2-dominant, isoprene-rich, with the presence of acidic particles in the submicron fraction of the atmospheric particle population. Factors OOA-2 and OOA-3 were identified in the patterns of the collected mass spectra. These factors were interpreted as tied to the in-basin production of biogenic secondary organic material and together accounted for >70% of the factor loadings, with the balance from HOA and OOA-1. The OOA-2 factor was implicated as associated with the reactive uptake of isoprene oxidation products, especially of epoxydiols to acidic haze, fog or cloud droplets. The OOA-3 factor was consistent with an association to the fresh production of SOM by a mechanism of gas-phase oxidation of BVOCs followed by gas-to-particle conversion of the oxidation products. Although multivariate statistical factors do not correspond to segregated individual chemical components (e.g., unlike molecules or families of molecules), the factors nevertheless can be indicative of the relative importance of different atmospheric emissions and process pathways. With this caveat in mind, the PMF analysis herein finds that the factor loadings were, on average, in a ratio of 1.4:1 for OOA-2 compared to OOA-3 and were alternately dominated in different periods of AMAZE-08 by the OOA-2 and OOA-3. These findings suggest a comparable importance of gas-phase and particle-phase (including haze, fog,

392 and cloud droplets) production of SOM during the study period.

Acknowledgments. Support was received from the USA National Science Foundation, the German Max Planck Society, and Brazilian CNPq and FAPESP agencies. QC acknowledges a NASA Earth and Space Science Fellowship. DKF acknowledges a NOAA Global Change Fellowship. TP acknowledges the CNPq grant 552831/2006-9. PA acknowledges FAPESP projects 2008/58100-2, 2010/52658-1, 2011/50170-4, 2012/14437-9. We thank the INPA LBA central office in Manaus for logistical support during AMAZE-08. We thank John Jayne, Joel Kimmel, Johannes Schneider, and Soeren Zorn for helping with sampling and aspects of data analysis.

References

Ahlm, L., Nilsson, E. D., Krejci, R., Martensson, E. M., Vogt, M., and Artaxo, P.: Aerosol number fluxes over the Amazon rain forest during the wet season, Atmos. Chem. Phys., 9, 9381-9400, 2009.

Aiken, A. C., Decarlo, P. F., Kroll, J. H., Worsnop, D. R., Huffman, J. A., Docherty, K. S., Ulbrich, I. M., Mohr, C., Kimmel, J. R., Sueper, D., Sun, Y., Zhang, Q., Trimborn, A., Northway, M., Ziemann, P. J., Canagaratna, M. R., Onasch, T. B., Alfarra, M. R., Prevot, A. S. H., Dommen, J., Duplissy, J., Metzger, A., Baltensperger, U., and Jimenez, J. L.: O/C and OM/OC ratios of primary, secondary, and ambient organic aerosols with high-resolution time-of-flight aerosol mass spectrometry, Environ. Sci. Technol., 42, 4478-4485, 10.1021/es703009q, 2008.

Andreae, M. O.: Aerosols before pollution, Science, 315, 50-51, 10.1126/science.1136529, 2007.

Andreae, M. O., Berresheim, H., Bingemer, H., Jacob, D. J., Lewis, B. L., Li, S. M., and Talbot, R. W.: The atmospheric sulfur cycle over the Amazon Basin. 2. Wet season, J. Geophys. Res., 95, 16813-16824, 1990.

Baars, H., Ansmann, A., Althausen, D., Engelmann, R., Artaxo, P., Pauliquevis, T., and Souza, R.: Further evidence for significant smoke transport from Africa to Amazonia, Geophys. Res. Lett., 38, L20802, 10.1029/2011GL049200, 2011.

Ben-Ami, Y., Koren, I., Rudich, Y., Artaxo, P., Martin, S. T., and Andreae, M. O.: Transport of North African dust from the Bodele depression to the Amazon Basin: a case study, Atmos. Chem. Phys., 10, 7533-7544, 10.5194/acp-10-7533-2010, 2010.

Budisulistiorini, S. H., Canagaratna, M. R., Croteau, P. L., Marth, W. J., Baumann, K., Edgerton, E. S., Shaw, S. L., Knipping, E. M., Worsnop, D. R., Jayne, J. T., Gold, A., and Surratt, J. D.: Real-time continuous characterization of secondary organic aerosol derived from isoprene epoxydiols in downtown Atlanta, Georgia, using the Aerodyne aerosol chemical speciation monitor, Environ. Sci. Technol., 47, 5686-5694, 10.1021/es400023n, 2013.

Canagaratna, M. R., Jayne, J. T., Ghertner, D. A., Herndon, S., Shi, Q., Jimenez, J. L., Silva, P. J., Williams, P., Lanni, T., Drewnick, F., Demerjian, K. L., Kolb, C. E., and Worsnop, D. R.: Chase studies of particulate emissions from in-use New York City vehicles, Aerosol Sci. Technol., 38, 555-573, Doi 10.1080/02786820490465504, 2004.

Canagaratna, M. R., Jimenez, J. L., Kroll, J. H., Chen, Q., Kessler, S. H., Massoli, P., Hildebrandt Ruiz, L., Fortner, E., Williams, L. R., Wilson, K. R., Surratt, J. D., Donahue, N. M., Jayne, J. T., and Worsnop, D. R.: Elemental ratio measurements of organic compounds using aerosol mass spectrometry: characterization, improved calibration, and implications, Atmos. Chem. Phys., 15, 253-272, 10.5194/acp-15-253-2015, 2015.

Chen, Q., Farmer, D. K., Schneider, J., Zorn, S. R., Heald, C. L., Karl, T. G., Guenther, A., Allan, J. D., Robinson, N., Coe, H., Kimmel, J. R., Pauliquevis, T., Borrmann, S., Pöschl, U., Andreae, M. O., Artaxo, P., Jimenez, J. L., and Martin, S. T.: Mass spectral characterization of submicron biogenic organic particles in the Amazon Basin, Geophys. Res. Lett., 36, L20806, 10.1029/2009gl039880, 2009.

Chen, Q., Liu, Y., Donahue, N. M., Shilling, J. E., and Martin, S. T.: Particle-phase chemistry of secondary organic material: Modeled compared to measured O:C and H:C elemental ratios provide constraints, Environ. Sci. Technol., 45, 4763-4770, 10.1021/es104398s, 2011.

Chen, Q., Li, Y. L., McKinney, K. A., Kuwata, M., and Martin, S. T.: Particle mass yield from β-caryophyllene ozonolysis, Atmos. Chem. Phys., 12, 3165-3179, 10.5194/acp-12-3165-2012, 2012.

Chirico, R., DeCarlo, P. F., Heringa, M. F., Tritscher, T., Richter, R., Prevot, A. S. H., Dommen, J., Weingartner, E., Wehrle, G., Gysel, M., Laborde, M., and Baltensperger, U.: Impact of aftertreatment devices on primary emissions and secondary organic aerosol formation potential from in-use diesel vehicles: results from smog chamber experiments, Atmos. Chem. Phys., 10, 11545-11563, 10.5194/acp-10-11545-2010, 2010.

Docherty, K. S., Aiken, A. C., Huffman, J. A., Ulbrich, I. M., DeCarlo, P. F., Sueper, D., Worsnop, D. R., Snyder, D. C., Peltier, R. E., Weber, R. J., Grover, B. D., Eatough, D. J., Williams, B. J., Goldstein, A. H., Ziemann, P. J., and Jimenez, J. L.: The 2005 Study of Organic Aerosols at Riverside (SOAR-1): instrumental intercomparisons and fine particle composition, Atmos. Chem. Phys., 11, 12387-12420, 10.5194/acp-11-12387-2011, 2011.

Ehn, M., Thornton, J. A., Kleist, E., Sipila, M., Junninen, H., Pullinen, I., Springer, M., Rubach, F., Tillmann, R., Lee, B., Lopez-Hilfiker, F., Andres, S., Acir, I. H., Rissanen, M., Jokinen, T., Schobesberger, S., Kangasluoma, J., Kontkanen, J., Nieminen, T., Kurten, T., Nielsen, L. B., Jorgensen, S., Kjaergaard, H. G., Canagaratna, M., Dal Maso, M., Berndt, T., Petaja, T., Wahner, A., Kerminen, V. M., Kulmala, M., Worsnop, D. R., Wildt, J., and Mentel, T. F.: A large source of low-volatility secondary organic aerosol, Nature, 506, 476-479, 10.1038/nature13032, 2014.

Elbert, W., Taylor, P. E., Andreae, M. O., and Pöschl, U.: Contribution of fungi to primary biogenic aerosols in the atmosphere: wet and dry discharged spores, carbohydrates, and inorganic ions, Atmos. Chem. Phys., 7, 4569-4588, 10.5194/acp-7-4569-2007, 2007.

Emanuelsson, E. U., Hallquist, M., Kristensen, K., Glasius, M., Bohn, B., Fuchs, H., Kammer, B., Kiendler-Scharr, A., Nehr, S., Rubach, F., Tillmann, R., Wahner, A., Wu, H. C., and Mentel, T. F.: Formation of anthropogenic secondary organic aerosol (SOA) and its influence on biogenic SOA properties, Atmos. Chem. Phys., 13, 2837-2855, 10.5194/acp-13-2837-2013, 2013.

Ervens, B., Turpin, B. J., and Weber, R. J.: Secondary organic aerosol formation in cloud droplets and aqueous particles (aqSOA): a review of laboratory, field and model studies, Atmos. Chem. Phys., 11, 11069-11102, 10.5194/acp-11-11069-2011, 2011.

Fuzzi, S., Decesari, S., Facchini, M. C., Cavalli, F., Emblico, L., Mircea, M., Andreae, M. O., Trebs, I., Hoffer, A., Guyon, P., Artaxo, P., Rizzo, L. V., Lara, L. L., Pauliquevis, T., Maenhaut, W., Raes, N., Chi, X. G., Mayol-Bracero, O. L., Soto-Garcia, L. L., Claeys, M., Kourtchev, I., Rissler, J., Swietlicki, E., Tagliavini, E., Schkolnik, G., Falkovich, A. H., Rudich, Y., Fisch, G., and Gatti, L. V.: Overview of the inorganic and organic composition of size-segregated aerosol in Rondonia, Brazil, from the biomass-burning period to the onset of the wet season, J. Geophys. Res., 112, D01201, 10.1029/2005JD006741, 2007.

Gerab, F., Artaxo, P., Gillett, R., and Ayers, G.: PIXE, PIGE and ion chromatography of aerosol particles from northeast Amazon Basin, Nucl Instrum Meth B, 136, 955-960, 1998.

Graham, B., Guyon, P., Taylor, P. E., Artaxo, P., Maenhaut, W., Glovsky, M. M., Flagan, R. C., and Andreae, M. O.: Organic compounds present in the natural Amazonian aerosol: Characterization by gas chromatography-mass spectrometry, J. Geophys. Res., 108, 4766, 10.1029/2003jd003990, 2003a.

Graham, B., Guyon, P., Maenhaut, W., Taylor, P. E., Ebert, M., Matthias-Maser, S., Mayol-Bracero, O. L., Godoi, R. H. M., Artaxo, P., Meixner, F. X., Moura, M. A. L., Rocha, C., Van Grieken, R., Glovsky, M. M., Flagan, R. C., and Andreae, M. O.: Composition and diurnal variability of the natural Amazonian aerosol, J. Geophys. Res., 108, 4765, 10.1029/2003JD004049, 2003b.

Gunthe, S. S., King, S. M., Rose, D., Chen, Q., Roldin, P., Farmer, D. K., Jimenez, J. L., Artaxo, P., Andreae, M. O., Martin, S. T., and Pöschl, U.: Cloud condensation nuclei in pristine tropical rainforest air of Amazonia: size-resolved measurements and modeling of atmospheric aerosol composition and CCN activity, Atmos. Chem. Phys., 9, 7551-7575, 10.5194/acp-9-7551-2009, 2009.

He, L. Y., Lin, Y., Huang, X. F., Guo, S., Xue, L., Su, Q., Hu, M., Luan, S. J., and Zhang, Y. H.: Characterization of high-resolution aerosol mass spectra of primary organic aerosol emissions from Chinese cooking and biomass burning, Atmos. Chem. Phys., 10, 11535-11543, DOI 10.5194/acp-10-11535-2010, 2010.

IPCC: *Climate Change 2013: The Physical Science Basis. Contribution of Working Group I to the Fifth Assessment Report of the Intergovernmental Panel on Climate Change* [Stocker, T.F., D. Qin, G.-K. Plattner, M. Tignor, S.K. Allen, J. Boschung, A. Nauels, Y. Xia, V. Bex and P.M. Midgley (eds.)], Cambridge University Press, Cambridge, United Kingdom and New York, NY, USA, 1535 pp, 2013.

Jimenez, J. L., Canagaratna, M. R., Donahue, N. M., Prevot, A. S. H., Zhang, Q., Kroll, J. H., DeCarlo, P. F., Allan, J. D., Coe, H., Ng, N. L., Aiken, A. C., Docherty, K. S., Ulbrich, I. M., Grieshop, A. P., Robinson, A. L., Duplissy, J., Smith, J. D., Wilson, K. R., Lanz, V. A., Hueglin, C., Sun, Y. L., Tian, J., Laaksonen, A., Raatikainen, T., Rautiainen, J., Vaattovaara, P., Ehn, M., Kulmala, M., Tomlinson, J. M., Collins, D. R., Cubison, M. J., Dunlea, E. J., Huffman, J. A., Onasch, T. B., Alfarra, M. R., Williams, P. I., Bower, K., Kondo, Y., Schneider, J., Drewnick, F., Borrmann, S., Weimer, S., Demerjian, K., Salcedo, D., Cottrell, L., Griffin, R., Takami, A., Miyoshi, T., Hatakeyama, S., Shimono, A., Sun, J. Y., Zhang, Y. M., Dzepina, K., Kimmel, J. R., Sueper, D., Jayne, J. T., Herndon, S. C., Trimborn, A. M., Williams, L. R., Wood, E. C., Middlebrook, A. M., Kolb, C. E., Baltensperger, U., and Worsnop, D. R.: Evolution of organic aerosols in the atmosphere, Science, 326, 1525-1529, 10.1126/science.1180353, 2009.

Karl, T., Guenther, A., Turnipseed, A., Tyndall, G., Artaxo, P., and Martin, S.: Rapid formation of isoprene photo-oxidation products observed in Amazonia, Atmos. Chem. Phys., 9, 7753-7767, 2009.

King, S. M., Rosenoern, T., Shilling, J. E., Chen, Q., Wang, Z., Biskos, G., McKinney, K. A., Pöschl, U., and Martin, S. T.: Cloud droplet activation of mixed organic-sulfate particles produced by the photooxidation of isoprene, Atmos. Chem. Phys., 10, 3953-3964, 10.5194/acp-10-3953-2010, 2010.

Kuhn, U., Ganzeveld, L., Thielmann, A., Dindorf, T., Schebeske, G., Welling, M., Sciare, J., Roberts, G., Meixner, F. X., Kesselmeier, J., Lelieveld, J., Kolle, O., Ciccioli, P., Lloyd, J., Trentmann, J., Artaxo, P., and Andreae, M. O.: Impact of Manaus City on the Amazon Green Ocean atmosphere: ozone production, precursor sensitivity and aerosol load, Atmos. Chem. Phys., 10, 9251-9282, 10.5194/acp-10-9251-2010, 2010.

Lambe, A. T., Onasch, T. B., Massoli, P., Croasdale, D. R., Wright, J. P., Ahern, A. T., Williams, L. R., Worsnop, D. R., Brune, W. H., and Davidovits, P.: Laboratory studies of the chemical composition and cloud condensation nuclei (CCN) activity of secondary organic aerosol (SOA) and oxidized primary organic aerosol (OPOA), Atmos. Chem. Phys., 11, 8913-8928, 10.5194/acp-11-8913-2011, 2011.

Lim, Y. B., Tan, Y., Perri, M. J., Seitzinger, S. P., and Turpin, B. J.: Aqueous chemistry and its role in secondary organic aerosol (SOA) formation, Atmos. Chem. Phys., 10, 10521-10539, 10.5194/acp-10-10521-2010, 2010.

Lin, Y. H., Zhang, Z. F., Docherty, K. S., Zhang, H. F., Budisulistiorini, S. H., Rubitschun, C. L., Shaw, S. L., Knipping, E. M., Edgerton, E. S., Kleindienst, T. E., Gold, A., and Surratt, J. D.: Isoprene epoxydiols as precursors to secondary organic aerosol formation: Acid-catalyzed reactive uptake studies with authentic compounds, Environ. Sci. Technol., 46, 250-258, 10.1021/es202554c, 2012.

Liu, Y. J., Herdlinger-Blatt, I., McKinney, K. A., and Martin, S. T.: Production of methyl vinyl ketone and methacrolein via the hydroperoxyl pathway of isoprene oxidation, Atmos. Chem. Phys., 13, 5715-5730, 10.5194/acp-13-5715-2013, 2013.

Liu, Y., Kuwata, M., Strick, B. F., Geiger, F. M., Thomson, R. J., McKinney, K. A., and Martin, S. T.: Uptake of epoxydiol isomers accounts for half of the particle-phase material produced from isoprene photooxidation via the HO2 pathway, Environ. Sci. Technol., 49, 250-258, 10.1021/es5034298, 2014.

Malm, W. C., Sisler, J. F., Huffman, D., Eldred, R. A., and Cahill, T. A.: Spatial and seasonal trends in particle concentration and optical extinction in the united states, J. Geophys. Res., 99, 1347-1370, 1994.

Martin, S. T., Andreae, M. O., Artaxo, P., Baumgardner, D., Chen, Q., Goldstein, A. H., Guenther, A., Heald, C. L., Mayol-Bracero, O. L., McMurry, P. H., Pauliquevis, T., Pöschl, U., Prather, K. A., Roberts, G. C., Saleska, S. R., Dias, M. A. S., Spracklen, D. V., Swietlicki, E., and Trebs, I.: Sources and properties of amazonian aerosol particles, Reviews of Geophysics, 48, Rg2002, 10.1029/2008rg000280, 2010a.

Martin, S. T., Andreae, M. O., Althausen, D., Artaxo, P., Baars, H., Borrmann, S., Chen, Q., Farmer, D. K., Guenther, A., Gunthe, S. S., Jimenez, J. L., Karl, T., Longo, K., Manzi, A., Muller, T., Pauliquevis, T., Petters, M. D., Prenni, A. J., Pöschl, U., Rizzo, L. V., Schneider, J., Smith, J. N., Swietlicki, E., Tota, J., Wang, J., Wiedensohler, A., and Zorn, S. R.: An overview of the Amazonian Aerosol Characterization Experiment 2008 (AMAZE-08), Atmos. Chem. Phys., 10, 11415-11438, 10.5194/acp-10-11415-2010, 2010b.

Matthew, B. M., Middlebrook, A. M., and Onasch, T. B.: Collection efficiencies in an Aerodyne aerosol mass spectrometer as a function of particle phase for laboratory generated aerosols, Aerosol Sci. Technol., 42, 884-898, 10.1080/02786820802356797, 2008.

Ng, N. L., Canagaratna, M. R., Zhang, Q., Jimenez, J. L., Tian, J., Ulbrich, I. M., Kroll, J. H., Docherty, K. S., Chhabra, P. S., Bahreini, R., Murphy, S. M., Seinfeld, J. H., Hildebrandt, L., Donahue, N. M., DeCarlo, P. F., Lanz, V. A., Prevot, A. S. H., Dinar, E., Rudich, Y., and Worsnop, D. R.: Organic aerosol components observed in Northern Hemispheric datasets from Aerosol Mass Spectrometry, Atmos. Chem. Phys., 10, 4625-4641, 10.5194/acp-10-4625-2010, 2010.

Ng, N. L., Canagaratna, M. R., Jimenez, J. L., Chhabra, P. S., Seinfeld, J. H., and Worsnop, D. R.: Changes in organic aerosol composition with aging inferred from aerosol mass spectra, Atmos. Chem. Phys., 11, 6465-6474, 10.5194/acp-11-6465-2011, 2011.

Nguyen, T. B., Coggon, M. M., Bates, K. H., Zhang, X., Schwantes, R. H., Schilling, K. A., Loza, C. L., Flagan, R. C., Wennberg, P. O., and Seinfeld, J. H.: Organic aerosol formation from the reactive uptake of isoprene epoxydiols (IEPOX) onto non-acidified inorganic seeds, Atmos. Chem. Phys., 14, 3497-3510, 10.5194/acp-14-3497-2014, 2014.

Ortega, A. M., Day, D. A., Cubison, M. J., Brune, W. H., Bon, D., de Gouw, J. A., and Jimenez, J. L.: Secondary organic aerosol formation and primary organic aerosol oxidation from biomass burning smoke in a flow reactor during FLAME-3, Atmos. Chem. Phys., 13, 11551-11571, 10.5194/acp-13-11551-2013, 2013.

Paatero, P., and Tapper, U.: Positive matrix factorization - a nonnegative factor model with optimal utilization of error-estimates of data values, Environmetrics, 5, 111-126, 10.1002/env.3170050203, 1994.

Pankow, J. F.: An absorption-model of the gas aerosol partitioning involved in the formation of secondary organic aerosol, Atmos. Environ., 28, 189-193, 1994.

Petzold, A., Kramer, H., and Schonlinner, M.: Continuous measurement of atmospheric black carbon using a multi-angle absorption photometer, Environmental Science and Pollution Research, 4, 78-82, 2002.

Pöhlker, C., Wiedemann, K. T., Sinha, B., Shiraiwa, M., Gunthe, S. S., Smith, M., Su, H., Artaxo, P., Chen, Q., Cheng, Y. F., Elbert, W., Gilles, M. K., Kilcoyne, A. L. D., Moffet, R. C., Weigand, M., Martin, S. T., Poeschl, U., and Andreae, M. O.: Biogenic potassium salt particles as seeds for secondary organic aerosol in the Amazon, Science, 337, 1075-1078, 10.1126/science.1223264, 2012.

Pöschl, U., Martin, S. T., Sinha, B., Chen, Q., Gunthe, S. S., Huffman, J. A., Borrmann, S., Farmer, D. K., Garland, R. M., Helas, G., Jimenez, J. L., King, S. M., Manzi, A., Mikhailov, E., Pauliquevis, T., Petters, M. D., Prenni, A. J., Roldin, P., Rose, D., Schneider, J., Su, H., Zorn, S. R., Artaxo, P., and Andreae, M. O.: Rainforest aerosols as biogenic nuclei of clouds and precipitation in the Amazon, Science, 329, 1513-1516, 10.1126/science.1191056, 2010.

Prenni, A. J., Petters, M. D., Kreidenweis, S. M., Heald, C. L., Martin, S. T., Artaxo, P., Garland, R. M., Wollny, A. G., and Pöschl, U.: Relative roles of biogenic emissions and Saharan dust as ice nuclei in the Amazon basin, Nature Geoscience, 2, 401-404, Doi 10.1038/Ngeo517, 2009.

Rizzo, L. V., Artaxo, P., Muller, T., Wiedensohler, A., Paixao, M., Cirino, G. G., Arana, A., Swietlicki, E., Roldin, P., Fors, E. O., Wiedemann, K. T., Leal, L. S. M., and Kulmala, M.: Long term measurements of aerosol optical properties at a primary forest site in Amazonia, Atmos. Chem. Phys., 13, 2391-2413, 10.5194/acp-13-2391-2013, 2013.

Robinson, N. H., Hamilton, J. F., Allan, J. D., Langford, B., Oram, D. E., Chen, Q., Docherty, K., Farmer, D. K., Jimenez, J. L., Ward, M. W., Hewitt, C. N., Barley, M. H., Jenkin, M. E., Rickard, A. R., Martin, S. T., McFiggans, G., and Coe, H.: Evidence for a significant proportion of secondary organic aerosol from isoprene above a maritime tropical forest, Atmos. Chem. Phys., 11, 1039-1050, 10.5194/acp-11-1039-2011, 2011.

Schneider, J., Freutel, F., Zorn, S. R., Chen, Q., Farmer, D. K., Jimenez, J. L., Martin, S. T., Artaxo, P., Wiedensohler, A., and Borrmann, S.: Mass- spectrometric identification of primary biological particle markers and application to pristine submicron aerosol measurements in Amazonia, Atmos. Chem. Phys., 11, 11415-11429, 10.5194/acp-11-11415-2011, 2011.

Shilling, J. E., Chen, Q., King, S. M., Rosenoern, T., Kroll, J. H., Worsnop, D. R., DeCarlo, P. F., Aiken, A. C., Sueper, D., Jimenez, J. L., and Martin, S. T.: Loading-dependent elemental composition of α-pinene SOA particles, Atmos. Chem. Phys., 9, 771-782, 10.5194/acp-9-771-2009, 2009.

Slowik, J. G., Brook, J., Chang, R. Y. W., Evans, G. J., Hayden, K., Jeong, C. H., Li, S. M., Liggio, J., Liu, P. S. K., McGuire, M., Mihele, C., Sjostedt, S., Vlasenko, A., and Abbatt, J. P. D.: Photochemical processing of organic aerosol at nearby continental sites: contrast between urban plumes and regional aerosol, Atmos. Chem. Phys., 11, 2991-3006, DOI 10.5194/acp-11-2991-2011, 2011.

Surratt, J. D., Chan, A. W. H., Eddingsaas, N. C., Chan, M. N., Loza, C. L., Kwan, A. J., Hersey, S. P., Flagan, R. C., Wennberg, P. O., and Seinfeld, J. H.: Reactive intermediates revealed in secondary organic aerosol formation from isoprene, Proc. Natl. Acad. Sci. U. S. A., 107, 6640-6645, 10.1073/pnas.0911114107, 2010.

Talbot, R. W., Andreae, M. O., Andreae, T. W., and Harriss, R. C.: Regional aerosol chemistry of the Amazon Basin during the dry season, J. Geophys. Res., 93, 1499-1508, 1988.

Talbot, R. W., Andreae, M. O., Berresheim, H., Artaxo, P., Garstang, M., Harriss, R. C., Beecher, K. M., and Li, S. M.: Aerosol chemistry during the wet season in central amazonia: The influence of long-range transport, J. Geophys. Res., 95, 16955-16969, 1990.

Trebs, I., Metzger, S., Meixner, F. X., Helas, G. N., Hoffer, A., Rudich, Y., Falkovich, A. H., Moura, M. A. L., da Silva, R. S., Artaxo, P., Slanina, J., and Andreae, M. O.: The NH_4^+-NO_3^--Cl^--SO_4^{2-}-H_2O aerosol system and its gas phase precursors at a pasture site in the Amazon Basin: How relevant are mineral cations and soluble organic acids?, J. Geophys. Res., 110, D07303, 10.1029/2004JD005478, 2005.

Ulbrich, I. M., Canagaratna, M. R., Zhang, Q., Worsnop, D. R., and Jimenez, J. L.: Interpretation of organic components from Positive Matrix Factorization of aerosol mass spectrometric data, Atmos. Chem. Phys., 9, 2891-2918, 2009.

Vaden, T. D., Imre, D., Beranek, J., Shrivastava, M., and Zelenyuk, A.: Evaporation kinetics and phase of laboratory and ambient secondary organic aerosol, Proc. Natl. Acad. Sci. U. S. A., 108, 2190-2195, 10.1073/pnas.1013391108, 2011.

Zhang, Q., Alfarra, M. R., Worsnop, D. R., Allan, J. D., Coe, H., Canagaratna, M. R., and Jimenez, J. L.: Deconvolution and quantification of hydrocarbon-like and oxygenated organic aerosols based on aerosol mass spectrometry, Environ. Sci. Technol., 39, 4938-4952, 10.1021/es048568l, 2005.

Zhang, Q., Jimenez, J. L., Canagaratna, M. R., Ulbrich, I. M., Ng, N. L., Worsnop, D. R., and Sun, Y. L.: Understanding atmospheric organic aerosols via factor analysis of aerosol mass spectrometry: a review, Anal. Bioanal. Chem., 401, 3045-3067, 10.1007/s00216-011-5355-y, 2011.

List of Figures

The NO_x concentration was measured as < 1 ppbv during these experiments and was estimated later as < 70 ppt for typical operating of the HEC (Liu et al., 2013). The relative intensities of ions having $m/z \geq 65$ were multiplied by 10. The intensities at each m/z represent three experiments that were performed at different SOM particle mass concentrations. A single intensity bar is color-coded by the contribution of different ion families (i.e., fragments containing C, H, O, or N for subscripts of x, y, z, $i \geq 1$) as determined from analysis of the high-resolution spectra (Shilling et al., 2009). The relative intensities of the $H_yO_1^+$ family were derived from the intensity of CO_2^+ based on calibrations described in Chen et al. (2011).

Figure 5. Statistical factors HOA, OOA-1, OOA-2, and OOA-3 identified by PMF analysis. The relative intensities of ions having $m/z \geq 65$ were multiplied by 10.

Figure 6. Time series of the loadings for the factors HOA, OOA-1, OOA-2, and OOA-3 (left axes; dots) and time series of the concentrations of tracer species, including NO_x, CO, AMS chloride, AMS potassium, aethalometer black-carbon, MVK + MACR, isoprene, monoterpenes, and sesquiterpenes (right axes; lines). The BVOCs were measured by PTR-MS (Karl et al., 2009).

Figure 7. Comparison of the OOA-3 factor to a synthetic mass spectrum obtained from a linear combination of the mass spectra of laboratory-generated biogenic SOM (30% α-pinene-derived SOM, 20% β-caryophylene-derived SOM, and 50% isoprene-derived SOM at mass concentrations of 0.4 to 0.7 $\mu g\ m^{-3}$).

Figure 8. Campaign-average diel profiles of the loadings of the factors HOA, OOA-1, OOA-2, and OOA-3.

Figure 9. (top) Mass-diameter distributions measured by the AMS and the daytime wind rose

for the two time periods shown in the bottom panel. (upper bottom) Time series of daily mean temperature measured at the top of the measurement tower TT34. (lower bottom) Time series of the fractional contribution by each of the four statistical factors identified by PMF analysis (left axes) and the rain counts (right axes). Two case periods that differ significantly in the fractional contribution of PMF factors are selected.

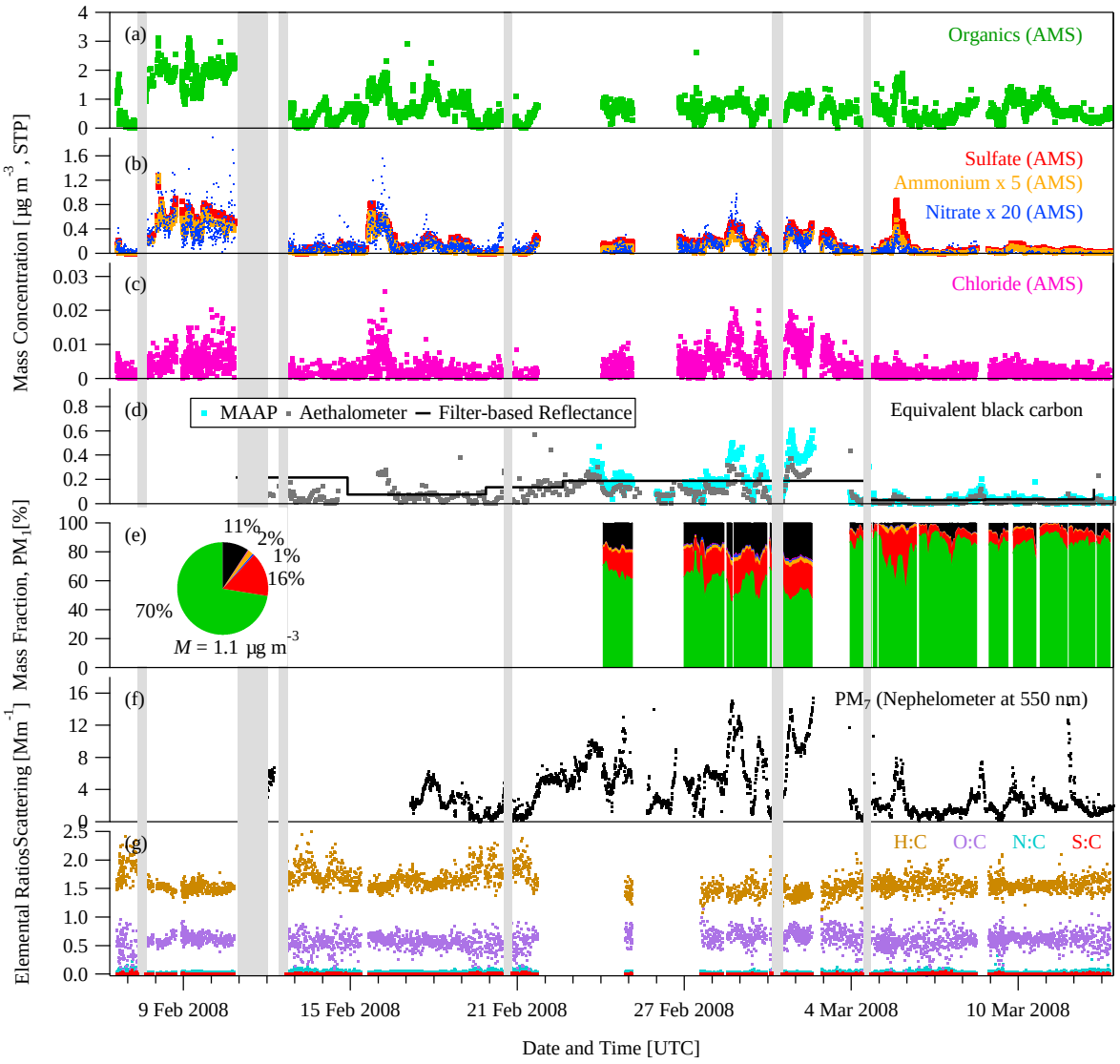
(a)
Organics (AMS)
(b)
Sulfate (AMS)
Ammonium x 5 (AMS)
Nitrate x 20 (AMS)
(c)
Chloride (AMS)
(d)
MAAP
Aethalometer
Filter-based Reflectance
Equivalent black carbon
(e)
11%
2%
1%
16%
70%
M = 1.1 µg m-3
(f)
PM7 (Nephelometer at 550 nm)
(g)
H:C
O:C
N:C
S:C
Mass Concentration [µg m-3, STP]
Mass Fraction, PM1 [%]
Scattering [Mm-1]
Elemental Ratios
9 Feb 2008
15 Feb 2008
21 Feb 2008
27 Feb 2008
4 Mar 2008
10 Mar 2008
Date and Time [UTC]

Figure 1

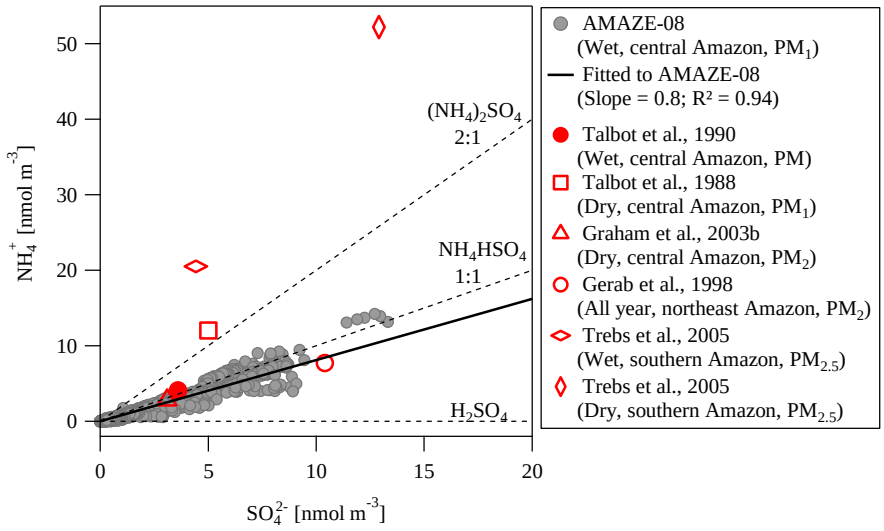
50
40
30
20
10
0
0
5
10
15
20
NH_4^+ [nmol m^{-3}]
SO_4^{2-} [nmol m^{-3}]
$(NH_4)_2SO_4$
2:1
NH_4HSO_4
1:1
H_2SO_4
AMAZE-08
(Wet, central Amazon, PM_1)
Fitted to AMAZE-08
(Slope = 0.8; R^2 = 0.94)
Talbot et al., 1990
(Wet, central Amazon, PM)
Talbot et al., 1988
(Dry, central Amazon, PM_1)
Graham et al., 2003b
(Dry, central Amazon, PM_2)
Gerab et al., 1998
(All year, northeast Amazon, PM_2)
Trebs et al., 2005
(Wet, southern Amazon, $PM_{2.5}$)
Trebs et al., 2005
(Dry, southern Amazon, $PM_{2.5}$)

Figure 2

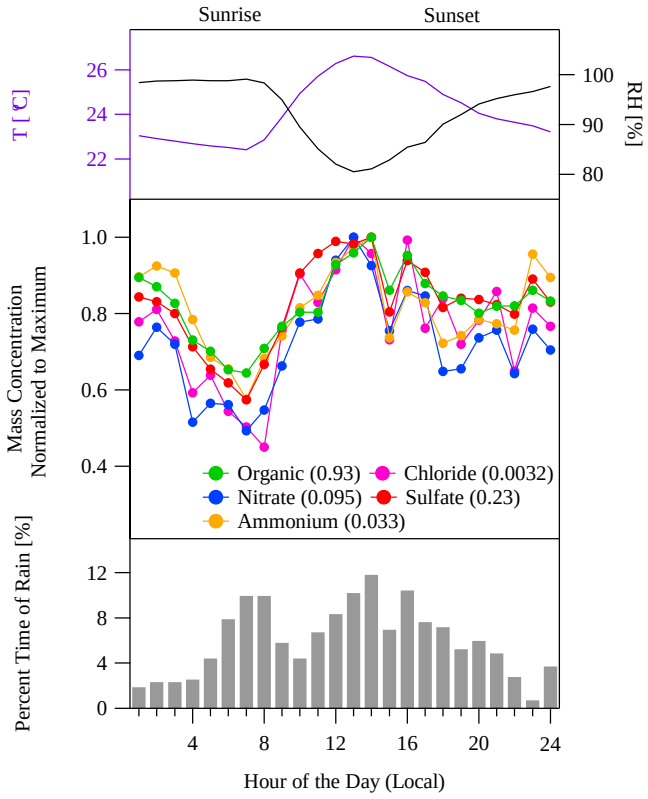
Sunrise
Sunset
T [°C]
26
24
22
RH [%]
100
90
80
Mass Concentration
Normalized to Maximum
1.0
0.8
0.6
0.4
Organic (0.93)
Chloride (0.0032)
Nitrate (0.095)
Sulfate (0.23)
Ammonium (0.033)
Percent Time of Rain [%]
12
8
4
0
4
8
12
16
20
24
Hour of the Day (Local)

Figure 3

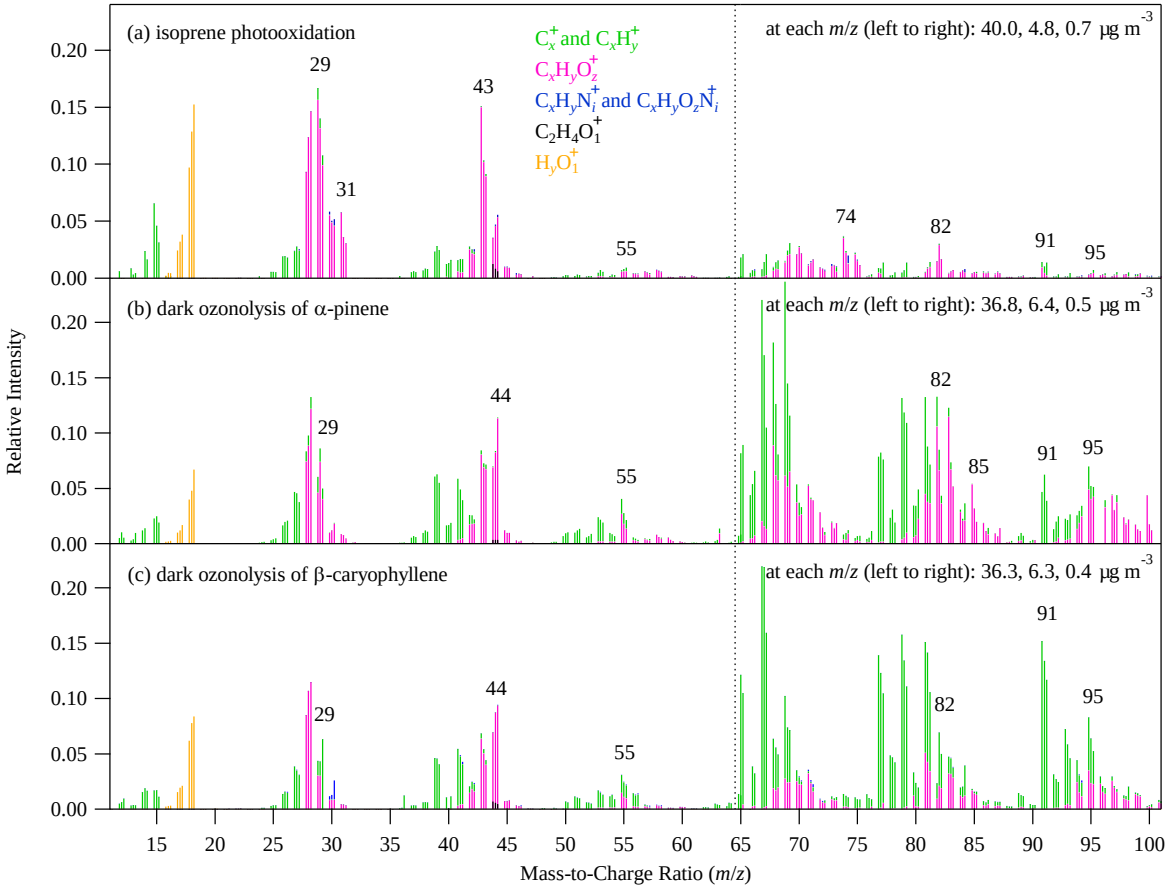
(a) isoprene photooxidation
C_x^+ and $C_xH_y^+$
$C_xH_yO_z^+$
$C_xH_yN_i^+$ and $C_xH_yO_zN_i^+$
$C_2H_4O_1^+$
$H_yO_1^+$
at each m/z (left to right): 40.0, 4.8, 0.7 μg m-3
(b) dark ozonolysis of α-pinene
at each m/z (left to right): 36.8, 6.4, 0.5 μg m-3
(c) dark ozonolysis of β-caryophyllene
at each m/z (left to right): 36.3, 6.3, 0.4 μg m-3
Relative Intensity
Mass-to-Charge Ratio (m/z)

Figure 4

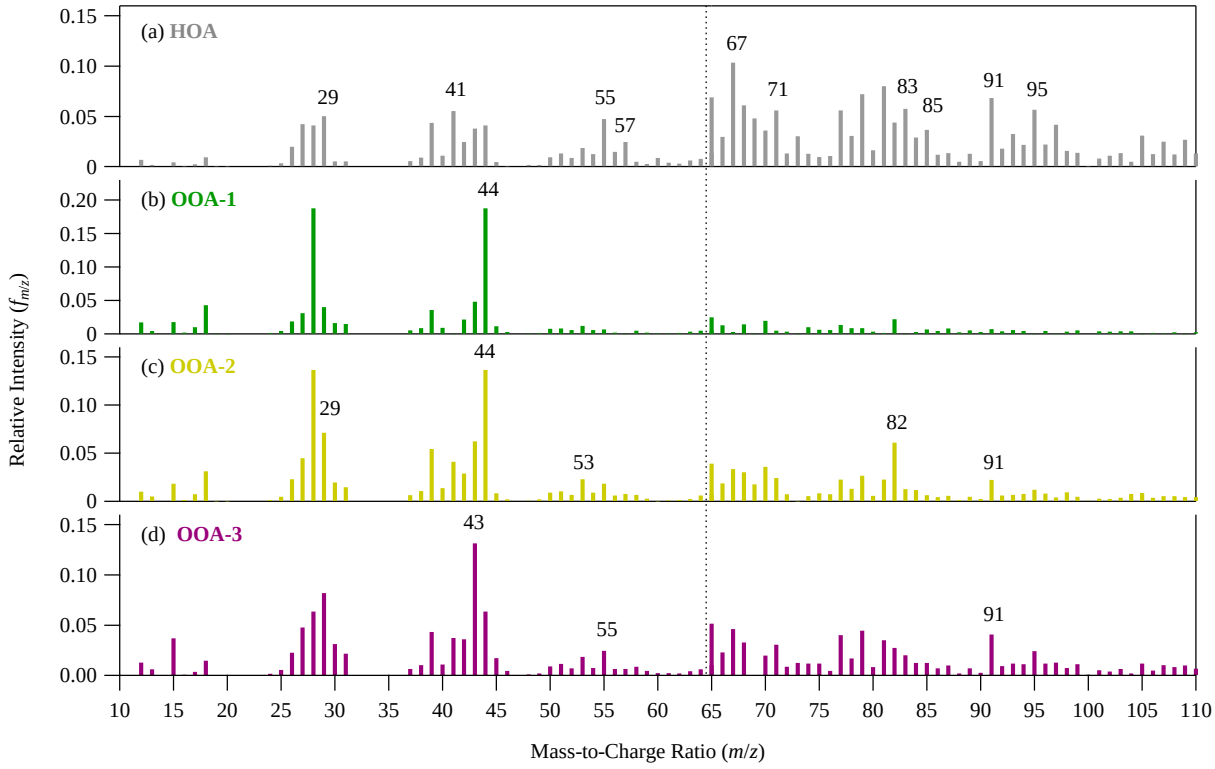
(a) HOA
(b) OOA-1
(c) OOA-2
(d) OOA-3
Relative Intensity ($f_{m/z}$)
Mass-to-Charge Ratio (m/z)

Figure 5

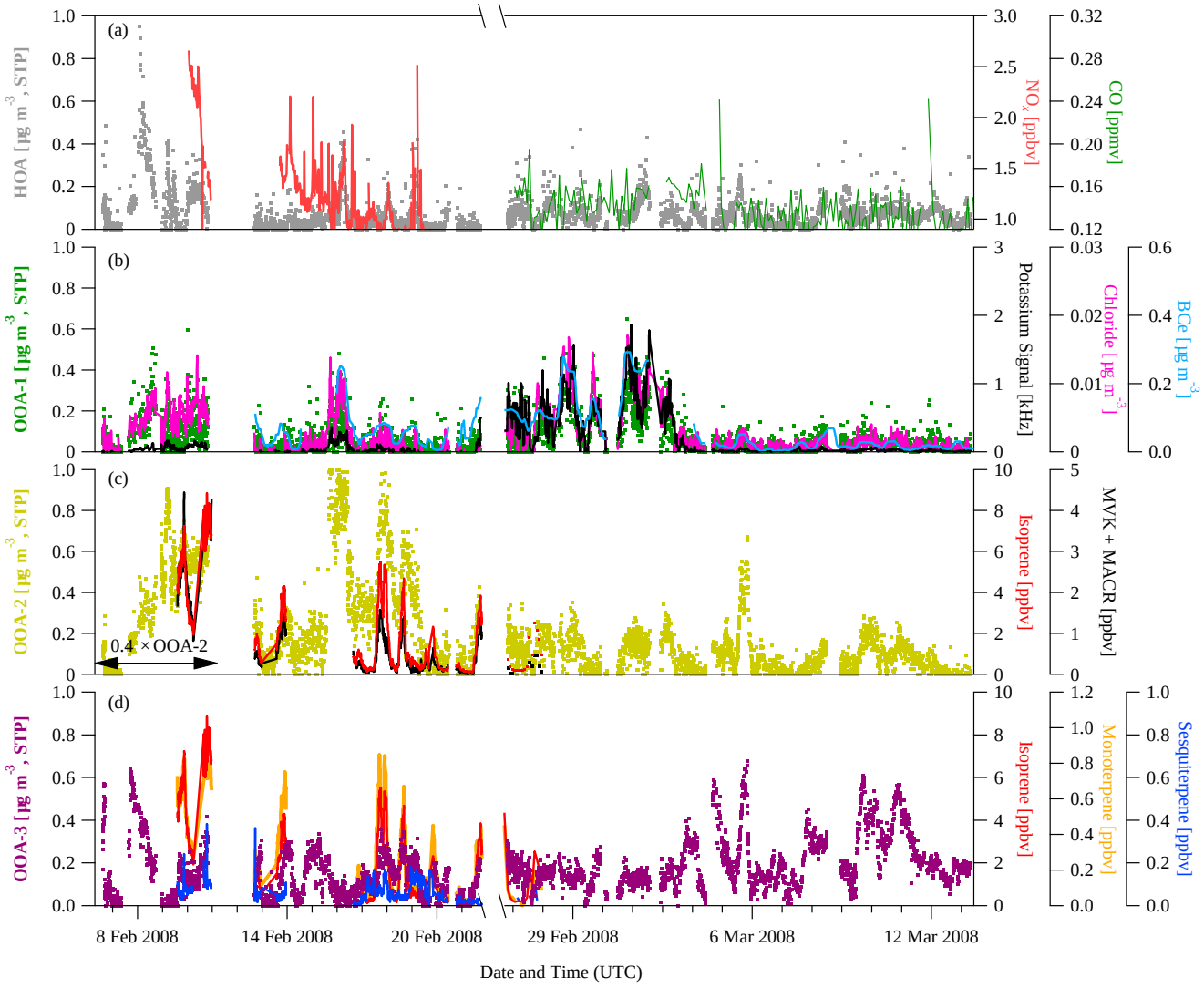
(a)
HOA [μg m-3, STP]
NOx [ppbv]
CO [ppmv]
(b)
OOA-1 [μg m-3, STP]
Potassium Signal [kHz]
Chloride [μg m-3]
BCe [μg m-3]
(c)
OOA-2 [μg m-3, STP]
0.4 × OOA-2
Isoprene [ppbv]
MVK + MACR [ppbv]
(d)
OOA-3 [μg m-3, STP]
Isoprene [ppbv]
Monoterpene [ppbv]
Sesquiterpene [ppbv]
8 Feb 2008
14 Feb 2008
20 Feb 2008
29 Feb 2008
6 Mar 2008
12 Mar 2008
Date and Time (UTC)

Figure 6

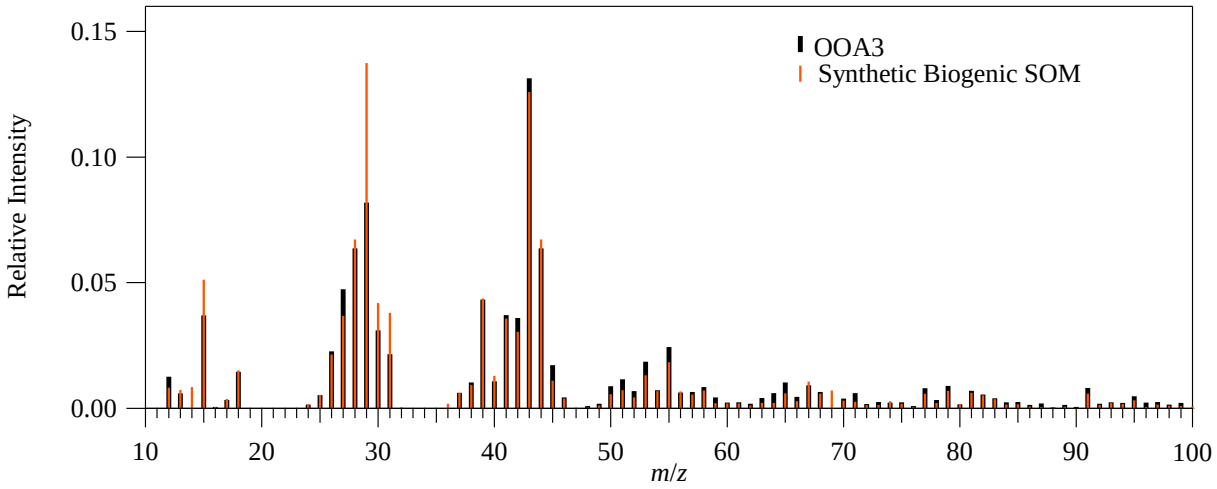
OOA3
Synthetic Biogenic SOM
Relative Intensity
0.15
0.10
0.05
0.00
10
20
30
40
50
60
70
80
90
100
m/z

Figure 7

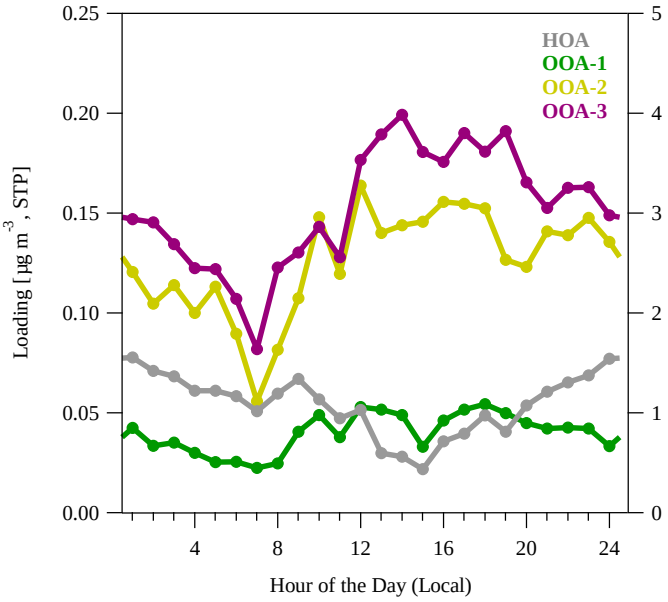
HOA
OOA-1
OOA-2
OOA-3
Loading [µg m-3 , STP]
Hour of the Day (Local)
0.25
0.20
0.15
0.10
0.05
0.00
5
4
3
2
1
0
4
8
12
16
20
24

Figure 8

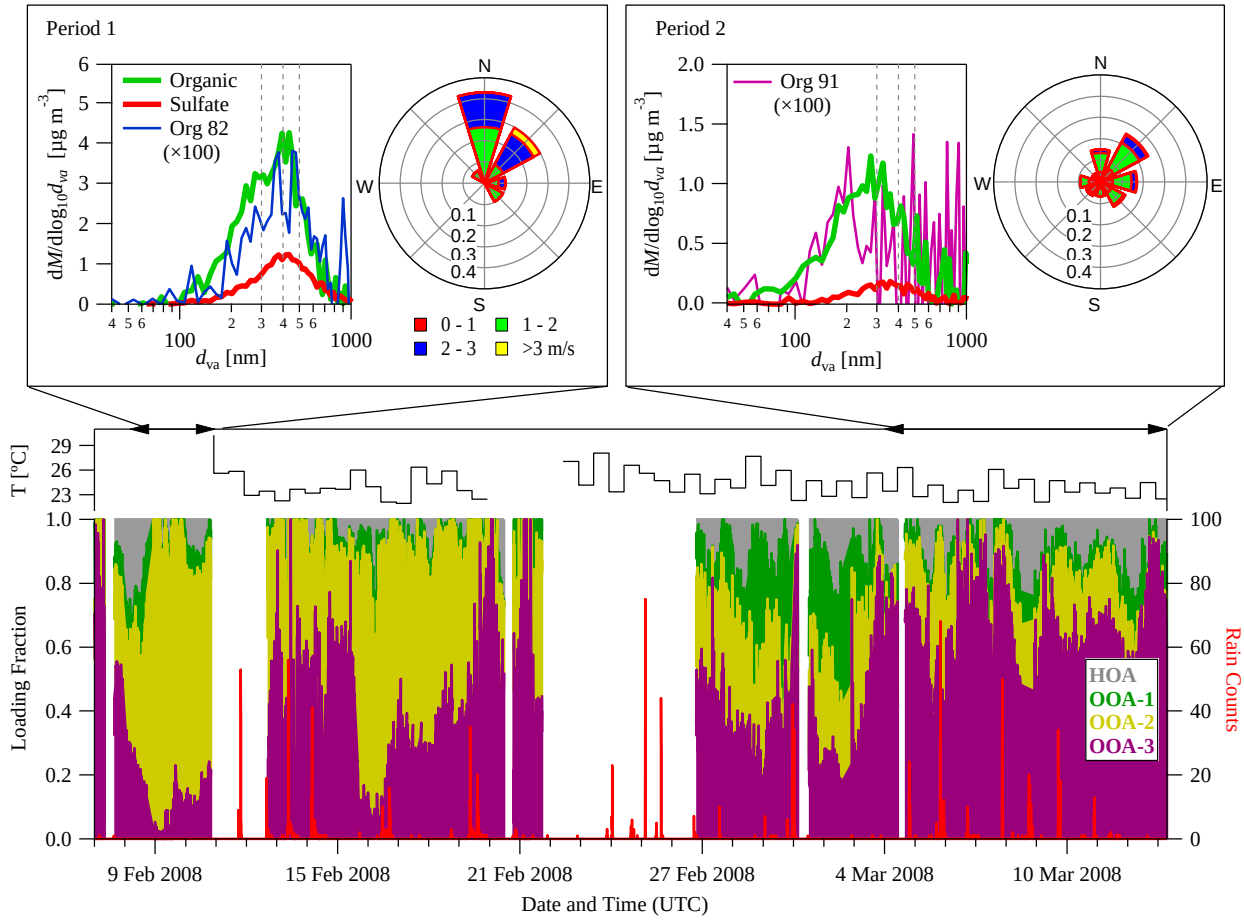
Period 1
Organic
Sulfate
Org 82
(×100)
dM/dlog10dva [µg m-3]
dva [nm]
N
W
E
S
0.1
0.2
0.3
0.4
0 - 1
1 - 2
2 - 3
>3 m/s
Period 2
Org 91
(×100)
T [ºC]
Loading Fraction
Rain Counts
HOA
OOA-1
OOA-2
OOA-3
9 Feb 2008
15 Feb 2008
21 Feb 2008
27 Feb 2008
4 Mar 2008
10 Mar 2008
Date and Time (UTC)

Figure 9